ACS OMEGA

Open Access

http://pubs.acs.org/journal/acsodf

Article

Bottom-Up Then Top-Down Synthesis of Gold Nanostructures Using Mesoporous Silica-Coated Gold Nanorods

Kristin A. Peck, Jennifer Lien, Mengqi Su, Aaron D. Stacy, and Ting Guo*

Cite This: *ACS Omega* 2023, 8, 42667−42677

Read Online

ACCESS | Metrics & More | Article Recommendations | Supporting Information

ABSTRACT: Gold nanostructures were synthesized by etching away gold from heat-treated mesoporous silica-coated gold nanorods (AuNR@mSiO_2), providing an example of top-down modification of nanostructures made using bottom-up methodology. Twelve different types of nanostructures were made using this **b**ottom-**u**p-**t**hen-**t**op-dow**n** **s**ynthesis (BUTTONS), of which the etching of the same starting nanomaterial of AuNR@mSiO_2 was found to be controlled by how AuNR@mSiO_2 were heat treated, the etchant concentration, and etching time. When the heat treatment occurred in smooth moving solutions in round-bottomed flasks, red-shifted longitudinal surface plasmon resonance (LSPR) was observed, on the order of 10−30 min, indicating increased aspect ratios of the gold nanostructures inside the mesoporous silica shells. When the heat treatment occurred in turbulent solutions in scintillation vials, a blue shift of the LSPR was obtained within a few minutes or less, resulting from reduced aspect ratios of the rods in the shells. The influence of the shape of the glassware, which may impact the flow patterns of the solution, on the heat treatment was investigated. One possible explanation is that the flow patterns affect the location of opened pores in the mesoporous shells, with the smooth flow of solution mainly removing CTAB surfactants from the pores along the cylindrical body of mSiO_2, therefore increasing the aspect ratios after etching, and the turbulent solutions removing more surfactants from the pores of the two ends or tips of the silica shells, hence decreasing the aspect ratios after etching. These new stable gold nanostructures in silica shells, bare and without surfactant protection, may possess unique chemical properties and capabilities. Catalysis using heat-treated nanomaterials was studied as an example of potential applications of these nanostructures.

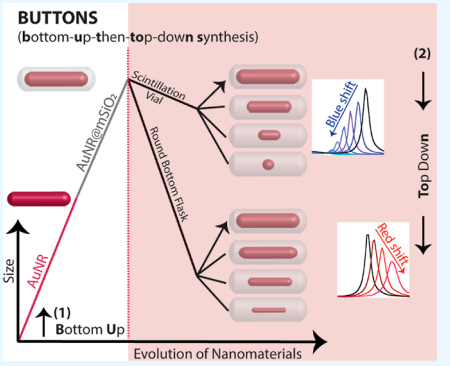

1. INTRODUCTION

There are two general methods of making nanostructures—bottom up and top down.[1] Bottom-up describes how to make larger nanostructures from smaller units, and top-down refers to making smaller nanostructures from larger ones.[2,3] The former is the synthesis of nanomaterials from ions, atoms, and molecules, and the latter refers to lithographically etching or breaking down large materials, such as bulk materials or films, into smaller nanoscale pieces.[4−6] More recently, a combination of the two has been used to make new nanomaterials.[7−9] For instance, nanocages have been used to form alloy nanocubes,[10] and nanowires have been made from nanorods.[11] This combined approach can be called BUTTONS, which stands for **b**ottom-**u**p **t**hen **t**op-dow**n** **s**ynthesis. The top-down part in BUTTONS could be direct chemical etching without lithography that employs e-beams.[12−14] Using chemical etching in solution is particularly attractive because often the nanostructures made from bottom-up methods are too small for e-beam-based etching. Direct chemical etching can be controlled with ligand coating.[15−17]

Gold nanorods (AuNRs) can be used to illustrate the working mechanisms of BUTTONS. The growth of AuNRs is well established and versatile, with control over their size, alloy, aspect ratio, and surfactants.[18−22] Direct etching of AuNRs using various etchants, such as I^-/H_2O_2, Fe^{3+}/H_2O_2, Fenton, Co^{2+}/Cu^{2+}, Pt, KCN, KSCN, e-beam, and light/laser/Fe^{3+}, have been studied,[23−31] and the etching is usually done in aqueous CTAB solution.[32]

There are several ways to monitor the evolution of BUTTONS. Transmission electron microscopy (TEM) can be used to monitor the etching, including that of individual AuNRs.[12,14] Another way to monitor or categorize BUTTONS is to study the bulk properties using UV−vis−NIR absorption spectroscopy,[33,34] which generally yields two possible spectroscopic end points—red or blue shift of its longitudinal surface plasmon resonance (LSPR) peaks. Most etching results showed blue-shifted LSPR peaks because the aspect ratio of the AuNRs was reduced.[33] There were also several reports showing a red shift of LSPR.[16,35−37] Beyond those two, there were reports that showed either red or blue shift from the same

Received: July 26, 2023
Revised: September 22, 2023
Accepted: October 17, 2023
Published: October 30, 2023

starting materials, depending on the etching conditions, including the intensity of the laser or the electron beam irradiating the AuNRs.[36,38,39] However, in those reports, either the end products were not shown, possibly because the etched products disappeared quickly or were in single AuNR etching conditions, or the red shift was insignificant.

Direct chemical etching can be controlled using surfactants coated on AuNRs. The literature-reported results suggest that for most ligands as surfactants, etching led to a blue shift—which was because there were more openings at tips of AuNRs due to low ligand densities at the tips.[15,40,41] However, some ligands such as peptide-coated AuNRs led to body etching, resulting in a red shift to the LSPR.[16] Another way to control the etching was to use hard shell coating such as mesoporous silica, which showed mostly a blue shift of the LSPR.[32,42,43] TEM was used to monitor the pores of the mesoporous shells in such etching and when the pores were more open, etching was more efficient.[42]

The products of BUTTONS can be used in many applications. For example, etching of AuNRs can be used as sensors to detect the etchant as the LSPR normally experiences a blue shift in response to etching.[34] A red shift in the LSPR after etching would make it more suitable for biomedical applications because of the water window up to 1000 nm.[44] Therefore, it is desirable to develop red-shifted LSPR associated with etching AuNR@mSiO$_2$. Furthermore, it may be possible to grow new structures from the etched Au nanostructures inside mesoporous shells,[45] as demonstrated with AuNRs.[11]

In all of these reports, a certain etching product can be made from a certain original nanostructure. There are yet no reports on large quantities of many different types of stable nanostructures made from the same starting nanomaterials for different applications, such as catalysis or colorimetric sensing. Here, a more systematic way to make many different stable nanostructures in large quantities was developed. The key to the working of BUTTONS was in the preparation of the reaction environment that facilitates the making of these new structures. The bottom-up part was represented by the synthesis of mesoporous silica coated gold nanorods (AuNR@mSiO$_2$).[18,43] The top-down part consisted of the treatment of AuNR@mSiO$_2$ in methanol at 60 °C in differently shaped containers, followed by etching with KCN (aq). The preetching heat treatment and subsequent etching resulted in nanostructures ranging from AuNRs with low and high aspect ratios to irregular gold nanostructures, to elongated or spherical gold nanoparticles, and to empty mesoporous silica shells. Depending on the treatment and etching, 12 different types of nanostructures or nanostructural end points were made. One of the advantages of the BUTTONS of these nanostructures is that bare and stable gold structures were created in the solvent without aggregation or precipitation.

Theoretical investigations using the discrete dipole approximation (DDA) method on the etched AuNR@mSiO$_2$ were carried out. DDA has been widely used to predict a LSPR shift as the aspect ratio of the AuNRs changes.[46] Simplification of nanostructures was adopted due to the complex shape evolution resulting from the outcome of the etching process. For instance, no finite element simulation of "dog biscuits" (vide infra) was carried out. In addition to the theoretical effort, mechanisms were investigated by studying the movement of the solution in different containers using optical microscopy. The evolution of the nanostructures was tracked by UV−vis−NIR absorption spectroscopy and TEM. Finally, a catalytic application was explored using the product of BUTTONS.

2. EXPERIMENTAL AND THEORETICAL METHODS

2.1. Chemicals. All chemicals were used without further purification. Hexadecyltrimethylammonium bromide (CTAB, ≥96%), gold(III) chloride solution in dilute HCl (HAuCl$_4$, 30 wt %), sodium hydroxide (97%), potassium cyanide, 4-nitrophenol, and sodium borohydride were purchased from Sigma-Aldrich. Sodium oleate (NaOL, 98%) was purchased from Tokyo Chemical Industry. Silver nitrate (AgNO$_3$, ≥99.9%) was purchased from Alfa Aesar. L-Ascorbic acid and methanol (99.8%) were obtained from Fisher Scientific. Tetraethyl orthosilicate (TEOS, 98%) was purchased from Acros Organics. Milli-Q Millipore water (MQ, 18.2 MΩ cm^{-1}) was used in all experiments. All glassware and magnetic stirring bars were cleaned with fresh aqua regia (HCl/HNO$_3$ in a 3:1 ratio by volume), rinsed with MQ water, and dried prior to use.

2.2. Syntheses. *2.2.1. Gold Nanorods (AuNRs).* AuNRs were synthesized using a previously established seeded growth method.[18] First, a growth solution was prepared by adding 7 g of CTAB and 1.234 g of sodium oleate to 250 mL of MQ water. After complete dissolution, the flask was equilibrated to 30 °C at which point 18 mL of a 4 mM AgNO$_3$ solution was added. The reaction was left without stirring for 15 min, after which 250 mL of 1 mM HAuCl$_4$ was added. The solution was left stirring at 300 rpm for 1.5 h. The seed solution was made by rapidly injecting 1 mL of an ice-cold freshly prepared 6 mM NaBH$_4$ solution into the vortex (1200 rpm) of a 10 mL mixture containing 0.25 mM HAuCl$_4$ and 0.1 M CTAB. After 2 min of stirring, the stir bar was removed, and the solution was aged at room temperature for 30 min. After 1.5 h of stirring, 1.5 mL concentrated HCl was added to the growth solution. After 15 min of slow stirring (300 rpm), 1.25 mL of 0.064 M ascorbic acid was introduced into the vortex (1000 rpm). 400 μL seed solution was immediately added to the solution. The growth solution was stirred vigorously for another minute before the stir bar was removed. Finally, the growth solution was left at 30 °C undisturbed for 12 h after which time the AuNRs were purified by centrifugation at 6000 rpm for 20 min and dispersed into 40 mL of water.

2.2.2. Silica-Coated Gold Nanorods (AuNR@mSiO$_2$). AuNRs in water were purified via centrifugation at 6000 rpm for 20 min. The pellet was redispersed in 60 mL of 1.7 mM CTAB and stirred for 15 min. The pH was adjusted within the range of 10.5−11 using 0.1 M sodium hydroxide (approximately 600 μL) for the CTAB-AuNRs. After stirring the mixture for 15 min, 20% TEOS in methanol was added dropwise via three additions of 180 μL, one addition every hour for 3 h. The solution was slowly stirred at room temperature for 2 days before being purified via centrifugation at 5200 rpm for 20 min and redispersed into methanol.[47]

2.2.3. Blue-Shifted LSPR: Heat Treatment and Oxidative Etching for AuNR@mSiO$_2$. AuNR@mSiO$_2$ was normalized to a 0.65 mM Au concentration via atomic absorption spectroscopy (AA). Heat treatment was carried out by heating the AuNR@mSiO$_2$ solution (5 mL in methanol) in a 25 mL scintillation vial (SV) at 60 °C for 20 min in a water bath. The solution was removed from the water bath and allowed to cool for 10 min with continuous stirring. The oxidative etching of AuNRs in mesoporous silica shells started with the addition of

https://doi.org/10.1021/acsomega.3c05444
ACS Omega 2023, 8, 42667−42677

KCN (aq). The concentration of KCN (0−2 mM) in a solution of AuNR@$mSiO_2$ was varied to control the etching speed. With the increase of etching time, the color of the solution changed from red, brown, green, blue, pink, and finally colorless within a few minutes. 200 μL aliquots were removed at the following color changes: green, blue, and pink. Each aliquot was diluted with 400 μL of methanol in an Eppendorf tube, followed by centrifugation at 4000 rpm for 5 min. The supernatant was removed, and samples were redispersed in 800 μL MeOH. Each time point was analyzed by UV−vis−NIR spectroscopy and TEM.

2.2.4. Red-Shifted LSPR: Heat Treatment and Oxidative Etching for AuNR@$mSiO_2$. This protocol was identical to "blue-shift" etching, except the heat treatment was performed in a 25 mL boiling flask containing 5 mL of AuNR@$mSiO_2$ in methanol. With the increase of etching time, the color of the solution changed from red to lighter brownish red until it was colorless. Aliquots of the solution were removed every 5 min until the solution was colorless to the naked eye. Each time point was analyzed by UV−vis−NIR spectroscopy and TEM.

2.2.5. Catalytic Reduction of 4-Nitrophenol. The catalytic properties of AuNR@$mSiO_2$ were carried out in a quartz cuvette by in situ monitoring of the UV−vis absorption of 4-nitrophenol in the presence of $NaBH_4$ at 400 nm.[48] For a typical catalysis experiment, 667.7 μL of 0.1 mM 4-nitrophenol solution was mixed with 67.7 μL of AuNR@$mSiO_2$ followed by the addition of 66.7 μL of freshly prepared ice cold 0.1 M $NaBH_4$. The Au concentration was normalized to 1 mM via AA at the start of each catalysis experiment. AuNR@$mSiO_2$ was prepared under three different conditions: no heat treatment, heat treatment in a SV, and heat treatment in a round-bottomed flask (RBF). The catalytic reduction was then monitored by observing the absorption at 400 nm with the use of UV−vis−NIR spectrophotometer. The peak at 400 nm, which corresponds to 4-nitrophenol, diminished, and a new peak at 300 nm formed as 4-aminophenol was produced over time.

2.3. Optical, Spectroscopic, Microscopic, and Theoretical Methods. *2.3.1. UV−Vis−NIR Spectroscopy.* All samples were measured with a Shimadzu UV-3600 UV−vis−NIR or a PerkinElmer Lambda 950 UV−vis−NIR spectrophotometer, using 1 mm quartz cuvettes.

2.3.2. Optical Microscopy Imaging Method. A 25 mL SV and a 50 mL two-necked RBF were used for the imaging of silica shells in solution. The SV was cut to a total height of 2 cm, and one of the necks of the RBF and roughly 2 cm length was removed. Synthesized mesoporous silica shells were prepared for imaging experiments. The imaging optics was a long working distance microscopic objective (Mitutoyo, M Plan Apo NIR 20×). A video camera (FLIR Blackfly S USB3) was used to capture the motion of the solutions. A green laser (Laser 301, 300 mW, 532 nm) was used to illuminate the solution. Frames of the movies were taken out and displayed in this work.

2.3.3. TEM Analysis. All samples were prepared by drop-casting a methanol or water solution containing nanostructures onto 300 mesh lacey carbon copper grids, the suspensions were dried. TEM images were taken using a Talos L120C instrument operating at 80 kV.

2.3.4. AA Spectroscopy. AA measurements were taken on a Varian/Spectra AA 220. The concentration of Au was determined prior to all of the etching and catalysis experiments.

2.3.5. DDA Analysis. The interaction between light and silica-coated gold nanorods was theoretically studied using the DDA method.[49] DDA method (version 7.3) was implemented by use of the open source nanoDDSCAT and nanoDDSCT+ tools (version 2.1b) available on nanoHUB. Object geometries for the silica-coated gold nanorods were generated using open-source Blender software based on experimental data obtained from TEM measurements. Dimensions for each structure were set to 1 Blender unit equal to 1 nm. The object file generated by Blender was converted into a shape file using the DDACONVERT tool, which can produce a 3D structure constructed from a cubic array of dipoles with a density of 1 dipole/nm. Contributions from ligands, such as CTAB, were not considered. The surrounding medium of refractive index for a vacuum and water was set to 1.0 and 1.33, respectively. The bulk experimental dielectric functions of Au and SiO_2 were taken from Johnson and Christy.[50] Lastly, the generated shape file was input into the DDSCAT tool and used to calculate the extinction efficiencies.

3. RESULTS AND DISCUSSION

3.1. Starting Materials for BUTTONS: AuNR@$mSiO_2$ (First Step of BUTTONS). The BUTTONS of nanomaterials started with making nanomaterials so that these nanomaterials can afford post modifications such as etching to create new nanomaterials. In this work, the starting materials were gold nanorods (AuNRs) (Figure 1A) and AuNRs coated with

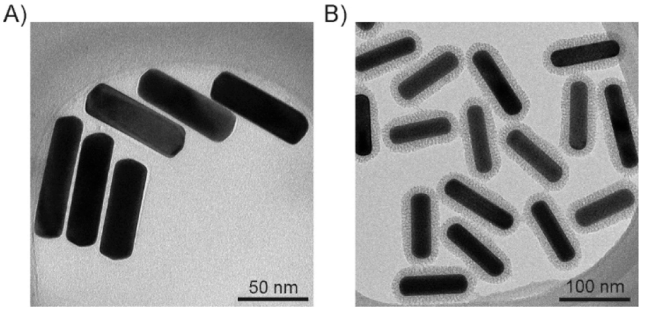

Figure 1. Starting nanomaterials of BUTTONS. (A) AuNRs. (B) AuNR@$mSiO_2$. The scale bars are 50 and 100 nm. Dimensions of AuNRs (109.5 ± 8.7 nm × φ33.9 ± 2.2 nm) and silica thickness (12.7 ± 1.9 nm) are given here.

mesoporous silica nanoshells (AuNR@$mSiO_2$) (Figure 1B). $mSiO_2$ provides a versatile chemical environment in which AuNRs can be etched while being protected by $mSiO_2$ to make the end product stable yet easy to use. The exact route of etching was determined by how $mSiO_2$ was treated prior to etching.

3.2. Heat Treatment of AuNR@$mSiO_2$ (Second Step of BUTTONS). AuNR@$mSiO_2$ were treated in 60 °C methanol for 20 min in two different types of glassware and TEM images are shown (Figure 2). AuNR@$mSiO_2$ before the heat treatment is also shown for comparison purpose (Figure 2A). AuNR@$mSiO_2$ after heat treatment in a flat bottom SV (Figure 2B) and in a RBF (Figure 2C) are shown. The treated AuNR@$mSiO_2$, AuNR@$mSiO_2$ (SV), and AuNR@$mSiO_2$ (RBF) were then purified and further modified under different etching conditions.

The TEM images of the AuNR@$mSiO_2$ before and after heat treatment show nearly identical AuNR nanostructures, similar to literature reported results.[42] However, the $mSiO_2$

https://doi.org/10.1021/acsomega.3c05444
ACS Omega 2023, 8, 42667−42677

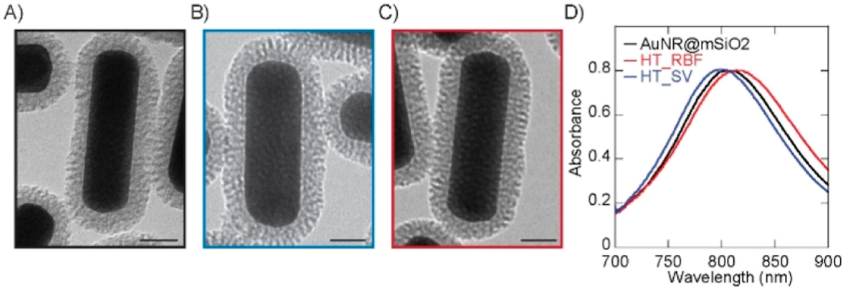

Figure 2. Heat treatment of AuNR@mSiO$_2$. (A) TEM (25 nm scale bar) images of before 20 min heat treatment for AuNR@mSiO$_2$, (B) 20 min heat treatment of AuNR@mSiO$_2$ in a SV, and (C) 20 min heat treatment of AuNR@SiO$_2$ in a RBF. (D) UV−vis−NIR spectra of heat treatment for AuNR@mSiO$_2$ before and after heat treatment in a SV and RBF. The colors of the panel frames shown in panels (A−C) correspond to the colors of the plots shown in (D).

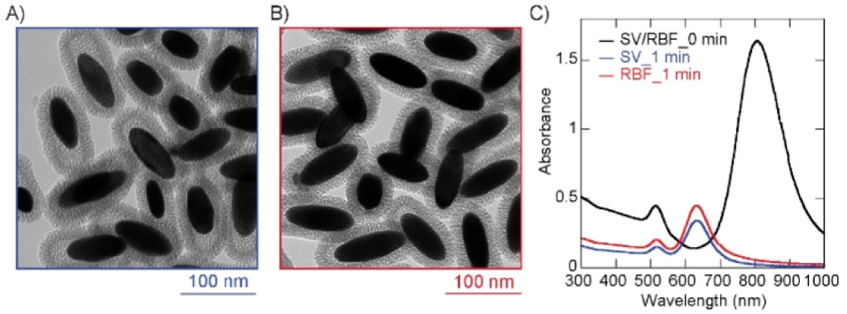

Figure 3. Etching without heat treatment in pure methanol. (A) TEM image (scale bar: 100 nm) of etching in SV for 1 min. (B) TEM image (scale bar: 100 nm) of etching in a RBF for 1 min. (C) UV−vis−NIR spectra of AuNR@mSiO$_2$ prior to etching (black), etching in a SV (blue), and etching in a RBF (red). Both etching products had their LSPR peaks blue-shifted. The colors of the panel frames shown in (A,B) correspond to the colors of the plots shown in (C).

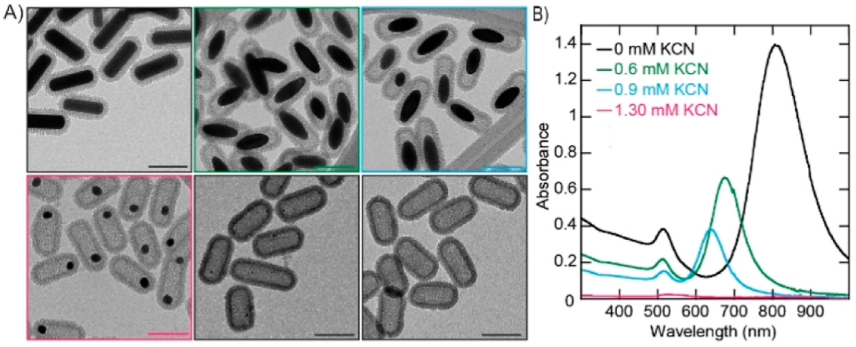

Figure 4. Summary of the etching results of AuNR@mSiO$_2$ after heat treatment in turbulent solutions in SV (normal conditions). (A) TEM images of the etched samples. The top three panels are, from left to right, the results of etching using KCN of 0, 0.6, and 0.9 mM, respectively. The bottom three panels, from left to right, are for 1.30, 1.6, and 2 mM KCN. The times taken by these etching were shorter than 1 min, often finished within less than a minute. The scale bars in the panels are 100 nm. (B) UV−vis−NIR absorption spectra of the etched samples. The colors of the panel frames shown in (A) correspond to the colors of the plots shown in (B).

pores before the heat treatment were more clogged with CTAB ligands, as shown in Figure 2A, than those shown in Figures 2B,C, with pores in Figure 2B (after heat treatment in SV) more open at the tips than those in Figure 2A (untreated) and 2C (after heat treatment in RBF). These differences led to different outcomes after etching (vide infra). This pore opening was also observed in other works.[42,51]

UV−vis−NIR absorption spectroscopy of the AuNR@mSiO$_2$ was measured with and without the heat treatment and in two different types of glassware (Figure 2D). A slight red shift of the LSPR peak (+10 nm, from 805 to 814 nm) was observed for AuNR@mSiO$_2$ heat treated in RBF, whereas a slight blue-shifted LSPR peak (−8 nm, from 805 to 797 nm) was observed when AuNR@mSiO$_2$ was heat treated in SV.

3.3. Etching of the Heat-Treated AuNR@mSiO$_2$ (The Third Step of BUTTONS). The silica shells created a unique chemical reaction environment that made the etching of AuNRs in them different from that of AuNRs alone. The latter was achieved by controlling the ligands on the AuNRs. The mesoporous silica shell provided AuNRs with a layer of protection, with the pores filled with CTAB ligands; etching occurred more efficiently if the pores were open after CTAB ligands were removed. Different shapes of the heat-treated glassware could lead to anisotropic etching that results in a red or blue shift of the LSPR peaks, representing the two spectroscopic end points available in this work and providing an advantage over other methods for directly etching AuNRs.

https://doi.org/10.1021/acsomega.3c05444
ACS Omega 2023, 8, 42667−42677

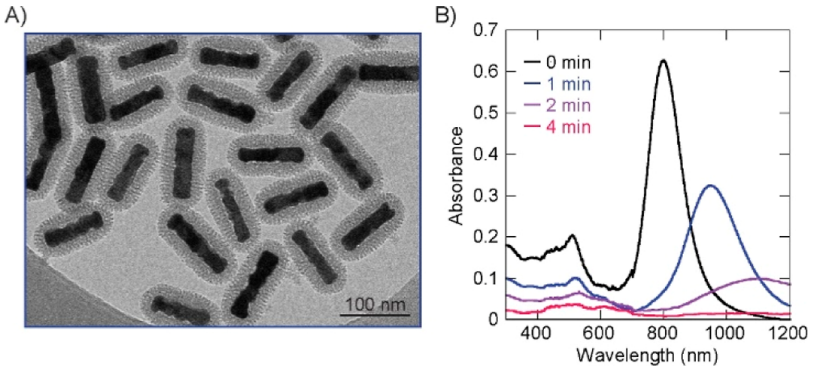

Figure 5. Etching of AuNR@mSiO$_2$ after heat treatment in nonturbulent solutions in SVs. (A) TEM image of the sample etched at 1.67 mM KCN (aq) for 1 min. Etching occurred most along the body of AuNRs. The scale bar is 100 nm. (B) UV−vis−NIR absorption spectra of the etched samples.

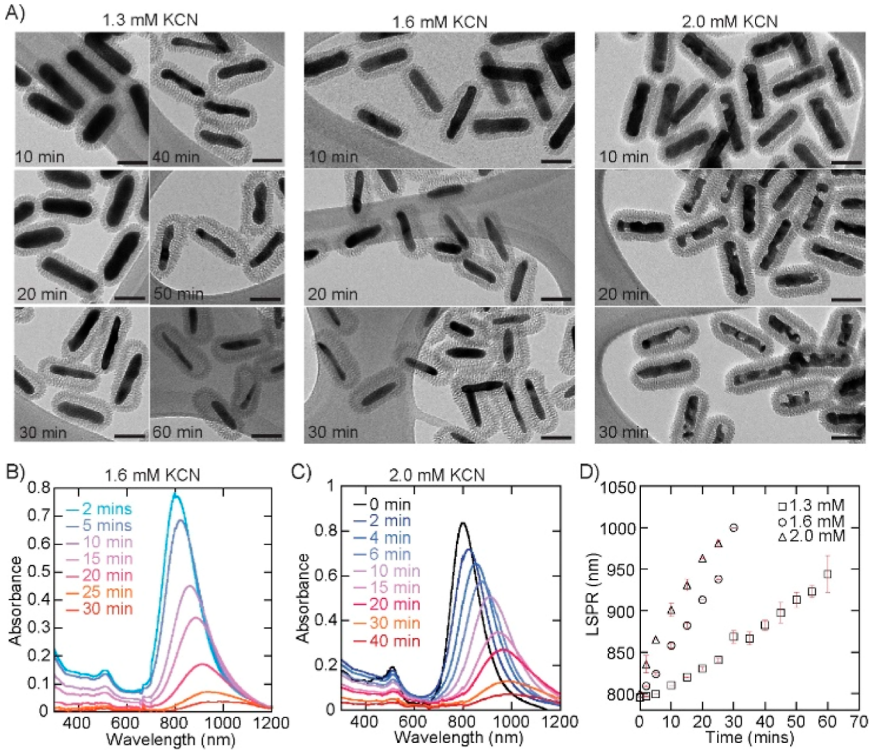

Figure 6. Etching of AuNR@mSiO$_2$ after heat treatment in RBF. (A) TEM images of KCN etched AuNR@mSiO$_2$. KCN concentrations (1.3, 1.6, and 2.0 mM) and etching times (10, 20, 30, and 60 min) are shown. For moderate concentrations (1.3 and 1.6 mM) of KCN, thin smooth AuNRs were made. For high concentrations (2.0 mM) of KCN, "dog-biscuit"-like gold nanostructures were made. (B) UV−vis−NIR spectra for 1.60 mM KCN. (C) UV−vis−NIR spectra for 2.0 mM KCN. (D) Data points for 1.30 mM (squares), 1.60 mM (circles), and 2 mM KCN (triangles) with error bars.

In addition to opening the pores uniformly or selectively, heat treatment has another function, which is to harden the silica nanoshells, especially when etching was performed in alcoholic solvents.[32,42]

3.3.1. Etching without Heat Treatment (for Comparison Purpose). Etching of AuNR@mSiO$_2$ in pure water, MeOH, and their mixtures without heat treatment was performed, and different results were obtained. In water, silica shells could not withstand etching without heat treatment. The silica wall shrunk when treated in hot water and then in room-temperature KCN (aq), similar to those reported in the literature.[32,42] When etching was carried out in pure MeOH, silica shells did not shrink.[32,42] After etching AuNR@mSiO$_2$ without heat treatment, Au was uniformly etched away in KCN (aq), leading to the blue-shifted LSPR (Figure 3A,B). Blue-shifted LSPR results were also observed with AuNR@mSiO$_2$ after etching in pure MeOH without heat treatment (Figure 3C). For comparison purposes, AuNRs were etched (Figure S1). The outcomes from etching in SV and RBF were similar, both resulting in a relatively uniform etching of AuNRs in mSiO$_2$.

3.3.2. Etching after Heat Treatment in SVs. In the SVs, in most cases, the stirring was visibly more turbulent than in RBFs, despite the stirring rates in these cases being similar. The heat treatment prior to etching in SV normally resulted in nanostructures with lower aspect ratios after etching (Figure 4A). The etching generally began with the loss of the tips of the AuNRs, and the AuNRs eventually became gold nano-

https://doi.org/10.1021/acsomega.3c05444
ACS Omega 2023, 8, 42667−42677

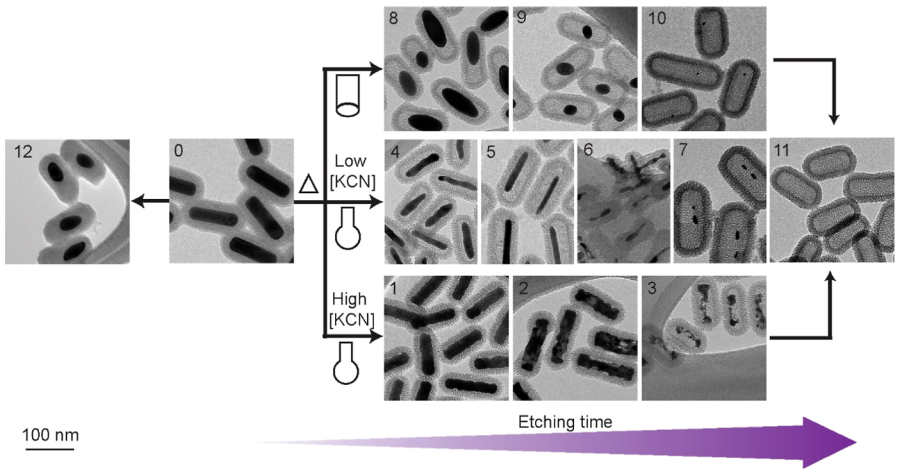

Figure 7. List of 12 (including the no heat treatment case) nanostructures made from the same starting nanomaterial of AuNR@$mSiO_2$, and the conditions of heat treatment and etching (KCN concentration and etching time). For etching in RBF, the concentration of KCN ranged from high (**1**−**3**) to low (**4**−**11**), and the time is shown on the horizontal axis. For etching in SV, the KCN concentration did not change the morphological evolution of the products (**8**−**10**). The soft shell (**12**)-wrapped Au nanostructures were obtained without heat treatment in a mixture of MeOH/water.

particles (AuNPs) after etching. The etching speed was fast, usually completed within 1 min, even at less than 1.0 mM KCN concentration (Figure 4). Small, <5 nm diameter, AuNPs in the $mSiO_2$ were observed. These AuNPs should not have any surfactants on their surface. Yet, they were stable and could not coalesce with other AuNPs due to the protection of the $mSiO_2$ shells. After extensive etching, AuNRs were completely etched away, leaving behind empty mesoporous silica nanoshells.

UV−vis−NIR responses were generally blue-shifted (Figure 4B). This trend matches the outcome of the trend reported in literature.[32,42,43,51] The absorbance decreased due to the diminished amount of Au over the course of etching. Nearly, a 200 nm blue shift was observed (Figure 4B).

However, occasionally the heat treatment in SV was nonturbulent, and under such conditions etching could result in red-shifted "dog-biscuit"-like nanostructures (Figure 5A). The change of the movement of the solution during heat treatment resulted in somewhat similar outcomes as coating the AuNRs with different surfactants, such as AuNRs coated with peptide−ethylene glycol (EG), which also caused a red shift of the plasmonic peak.[16,35−37] It is important to note that this result was not easily repeated. One of the reasons could be that the magnetic stir bar often jumped around during stirring to cause turbulent solution movement, so a long smooth motion of solution was difficult to achieve. TEM image of the etched AuNRs showed removal of Au on the body but not at the two ends of the AuNRs (Figure 5A).[23,52]

UV−vis−NIR responses of etching in the smooth solution in SV were red-shifted (Figure 5B). The absorbance decreased due to the diminishing amount of Au over the course of etching. Nearly, a 200 nm red shift was observed (Figure 5B).

3.3.3. Etching after Heat Treatment in Round-Bottomed Flasks. Etching after heat treatment of AuNR@$mSiO_2$ (stirring) in RBF was performed, and the results showed that the LSPR peaks experienced a red shift (Figure 6), which was the opposite to etching of AuNR@$mSiO_2$ in turbulent SVs (Figure 4). The etching of AuNR@$mSiO_2$ heat-treated in RBF began with the loss of Au on the body of AuNRs, which is different from what occurred to AuNRs in AuNR@$mSiO_2$ heat treated in turbulent SVs. In addition, the trend of the etching outcomes in RBF was independent of the stirring speed, which was observed in this work. This is unique because the etching was performed on the same starting nanomaterials of AuNR@$mSiO_2$; the only difference was the glassware in which AuNR@$mSiO_2$ was heat treated. It was observed that stirring in RBF normally generated a smoother moving solution that caused the pores along the body of AuNR@$mSiO_2$ to be more open due to the greater loss of ligands along the body.

KCN concentrations affected the speed and starting locations of etching and the morphology of the resulting products (Figure 6A). This is believed to be caused by fast etching of spots along the AuNR body. High concentrations of etchant resulted in "dog biscuits" (Figure 6A, third row) and low concentrations caused a higher aspect ratio but smooth-bodied AuNRs with thinner diameters or even wires (Figure 6A, first and second rows). This difference between low and high KCN concentrations may originate from the rate of etching—when it is too fast, etching results in local deep holes such as those shown in Figure 6A, third row. When the rate is slow, the etching causes larger patches of Au to be removed and when these patches are connected, a smooth body etching occurs, as shown in Figure 6A, first and second rows.

It is also noted that the times of etching in RBF were an order of magnitude or so slower than that in SV (even for the not so turbulent cases in SV), further demonstrating that the motion of the solution, which can be caused by the shape of the containers, exerted a major influence on the outcome of subsequent etching.

UV−vis−NIR responses of etching in smooth solution in RBF were nearly always red-shifted (Figure 6B,C). For a KCN concentration lower than 1.6 mM, the plasmonic profiles did not evolve beyond the envelope of the initial plasmonic profile of the unetched AuNR@$mSiO_2$ (Figure 6B). For 2.0 mM KCN, the plasmonic profiles of etched AuNR@$mSiO_2$ evolved beyond the initial envelope (Figure 6C). The absorbance decreased due to the loss of Au over the course of etching. Over 200 nm red shifts were observed (Figure 6B,C). The amount of red shift was displayed as well (Figure 6D). The rate of shift was higher for higher KCN concentrations.

3.3.4. Summary of the nanostructures Made Using BUTTONS. Collectively, 12 nanostructures were made through

https://doi.org/10.1021/acsomega.3c05444
ACS Omega 2023, 8, 42667−42677

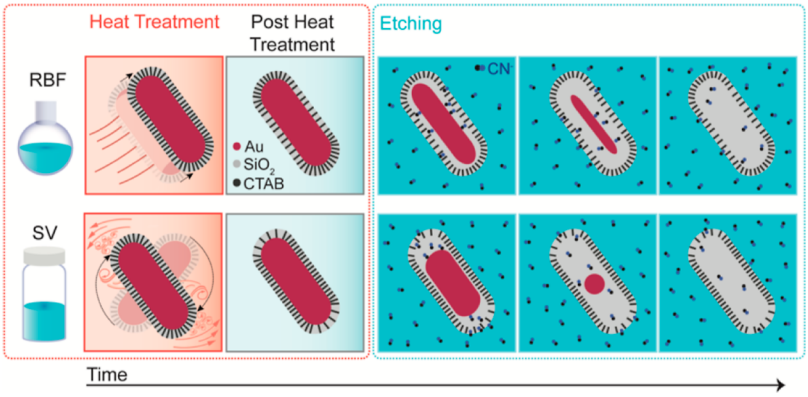

Figure 8. Illustration of how heat treatment in differently shaped containers affects the outcome of etching. The first two panels of the two rows show how heat-treatment in SV and RBF differentially removes CTAB ligands in the pores of AuNR@mSiO$_2$, with more CTAB ligands at the tips being removed than the body in the SV case and the CTAB ligands on the body of the AuNRs being removed more than the tips in the RBF case. Such treatments were caused by the motion of the solution in these two differently shaped containers, with RBF nearly always generating a smooth motion of solution and SV generating more frequently turbulent motion of solution. Once the pores are open, etching by KCN can be done more efficiently through those open pores, resulting in tip etching in SV and body etching in RBF.

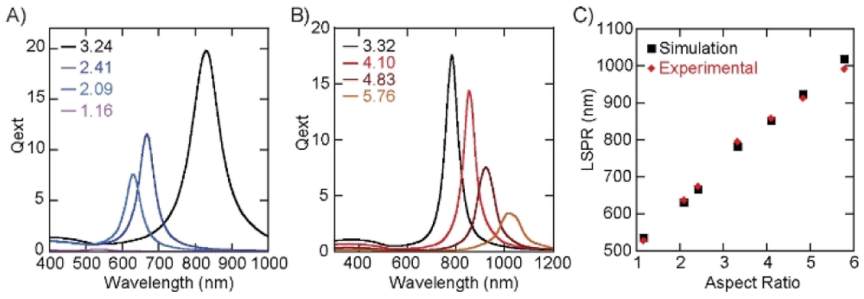

Figure 9. DDA simulation results are based on the shape obtained from the etching experiments. (A) Calculated extinction efficiencies (Qext) of the etched AuNR@mSiO$_2$ in SVs after heat treatment and (B) calculated Qext results of the etched AuNR@mSiO$_2$ in RBF after heat treatment. (C) LSPR as a function of the aspect ratio of results shown in A and B. The theoretical data points are taken from (A,B), and the experimental data points are taken in Figure 4 (blue-shifted) and Figure 6 (red-shifted).

etching of AuNR@mSiO$_2$ after heat treatment (Figure 7). These 12 nanostructures were obtained as the result of etching of the heat-treated AuNR@mSiO$_2$ with KCN (aq). The key was to maintain the silica shell structures by heat treatment while using the motion of the solution to selectively remove CTAB ligands in the pores of mesoporous silica shells. If the treatment was missing or incomplete, then mSiO$_2$ on the AuNRs was soft and would shrink as AuNRs inside were etched away, as shown in structure **12** in Figure 7.

The outcomes shown above represent an example of top-down modification after bottom-up syntheses, i.e., BUTTONS. The bottom-up step is nearly invariant in this work. All of the flexibility and variables were introduced during the top-down half of the synthetic processes. Additional controls such as heat treatment have been introduced on top of etching when the mesoporous silica shells are added into the equation or synthetic routes. Even the shape or the solution/liquid flow pattern has been shown to be able to influence the outcome, which is summarized in Figure 7.

Some of the nanomaterials presented here have been made in the past and reported in the literature, but not all of them existed before or have exhibited their properties in their pristine forms, as previously made nanostructures such as gold nanoparticles must be covered with large amounts of ligands to stay solvated in solvents. These ligands may negatively affect how these AuNRs can be used, as the ligands may hinder the movement of chemicals around AuNRs and hinder the access of chemicals to the surface of AuNRs. BUTTONS and these nanomaterials therefore offer a greater potential to make new nanomaterials, free of ligand protection, and to offer more applications.

The nanostructural end points shown in Figure 7 can be explained as follows (Figure 8). As show in the panels of Figure 8, the heat treatment in RBF generates smooth motion of the solution and therefore smooth motion of AuNR@mSiO$_2$ in solution. The rods move differently than the solvent due to the drag and other forces. In RBF, the relative motion is smooth, and most rods should have their body facing the motion of the solvent (first panel of the top row), as the AuNRs inside the shells are mainly body-etched because CN^- ions enter the shells through the pores along the body at the etching stage. Occasionally, solution motion in SV could be smooth and on those occasions, the etching starts from the body yet the speed is fast. For heat treatment in turbulent SVs, the AuNR@mSiO$_2$ tumbles in the solution (first panel of the bottom row) due to the turbulent motion of the solution in SV. Such movements lead to the tips of AuNR@mSiO$_2$ being more exposed to the solvent, causing loss of CTAB ligands from the pores at the tips of the AuNRs (and possibly around the body near the tips). In the etching stage, CN^- ions enter through the pores at the tips, leading to tip etching.

Although only 12 nanostructural end points and two spectroscopic end points, red and blue shifts of LSPR, are shown in this work, it is possible more end points are available.

https://doi.org/10.1021/acsomega.3c05444
ACS Omega 2023, 8, 42667−42677

For instance, conditions could result in a red shift, blue shift, no change as in LSPR remaining the same, or the profile of LSPR deviating significantly from the original. It is also possible that more nanostructures than the 12 shown here can be obtained. BUTTONS can then be used to control the end points of these syntheses. It is expected that BUTTONS may be used to control those potential and more complicated syntheses.

In the following, the theoretical method of the DDA was used to study the evolution of etching. Optical microscopy was used to study the mechanism of heat treatment and etching, and catalytic reactions were used to demonstrate the application potential of the nanomaterials made from BUTTONS.

3.4. Theoretical Investigation of AuNR@mSiO$_2$. The DDA method was used to study AuNR@mSiO$_2$ with different AuNRs shapes. DDA method has been widely used to study the plasmonic profiles of Au nanostructures, including AuNRs.[46,53−57]

Both blue and red shifts of the LSPR peak can be simulated by using the DDA method. AuNR@mSiO$_2$ construction used in the DDA simulation was shown in Figure S2. In these cases, the aspect ratio of the AuNRs determines the peak position. When the aspect ratio decreases, as shown in Figure 4, the peak experiences a blue shift (Figure 9A). When the aspect ratio increases as the AuNRs are thinned (Figure 6A), the peak experiences a red shift (Figure 9B). The magnitude of the red shift obtained with the DDA method was compared with that of the experimental values (Figures 4A and 6A), and the two trends were similar (Figure 9C).

3.5. Experimental Investigations of the Mechanisms of BUTTONS. Based on the literature discussion and the results shown above, it is believed that the reason for blue/red-shifted etching was caused by the pore opening in the mesoporous silica shells around AuNRs during the heat treatment. If the pores were filled with CTAB, then the etching would be slow. If the side pores were open by removing CTAB ligands at those locations, then etching was accelerated. During the heat treatment, which solidified the silica nanoshells as well as opened the pores, preferential pore opening determined the etching preference. If the end pores were more open, then blue-shifted LSPR occurred. If the pores along the body were more open, then red-shifted etching resulted. The shape of the glassware during the treatment was critical because it affected the motion of the solution and, therefore, the pore opening in the AuNR@mSiO$_2$. The following are the results of studying the heat treatment process.

The optical detection system (Figure 10A, left panel) was used to observe the solution in different types of glassware, as the motion is believed to be critical to determining the outcome of etching, as explained in Figure 8. The long working distance microscope objective was positioned close to the solution to observe the movement of the solution. Also shown are two frames of the videos: one for solution in SV (right top panel of Figure 10A) and one for solution in RBF (right bottom panel of Figure 10A). The solution in SV at 60 °C was apparently more turbulent than that in RBF at 60 °C, as more green scattering from the illuminating laser was observed from the solution in SV.

3.6. Applications of the nanomaterials Made from BUTTONS. BUTTONS of AuNR@mSiO$_2$ could have many potential applications. Here one of them is demonstrated briefly, which is the catalytic reduction of 4-nitrophenol to 4-aminophenol by AuNR@mSiO$_2$.

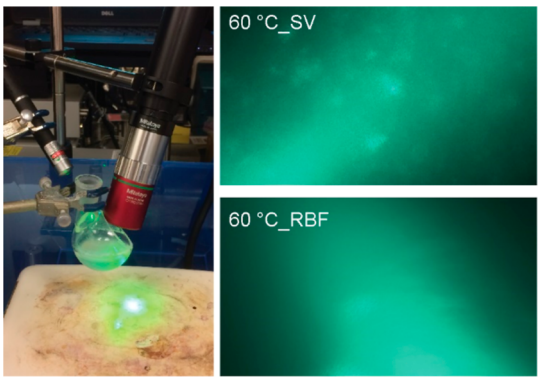

Figure 10. Analytical results of the investigations of the mechanisms of BUTTON synthesis. The experimental setup is shown in the left panel. Optical study of heat-treated AuNR@mSiO$_2$ in SV (top right panel) and RBF (bottom right panel) at 60 °C.

AuNRs and similar gold nanostructures have been studied for their catalytical properties[58−63] Here, AuNR@mSiO$_2$ were used as catalysts to study the reduction of 4-nitrophenol to 4-aminophenol in the presence of sodium borohydride.[48] The reduction was conducted using three samples: (1) AuNR@mSiO$_2$ without heat treatment; (2) AuNR@mSiO$_2$ with heat treatment in SV; and (3) AuNR@mSiO$_2$ with heat treatment in RBF. A typical response is shown in Figure 11A, which

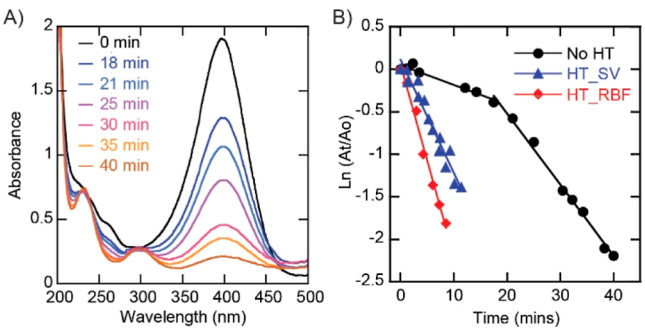

Figure 11. Catalytic reaction was studied using AuNR@mSiO$_2$. (A) UV−vis spectra for reduction of 4-nitrophenol to 4-aminophenol in the presence of sodium borohydride when AuNR@mSiO$_2$ was prepared without any heat treatment. (B) Catalysis of AuNR@mSiO$_2$ prepared without any heat treatment (black circles) and of AuNR@mSiO$_2$ prepared with heat treatment (no etching) in a SV (blue triangles) and RBF (red diamonds).

shows that the peak at 400 nm decreased over time and nearly completely disappeared after 40 min (Figure 11A). When AuNR@mSiO$_2$ were used, the rate of reaction accelerated (Figure 11B). For AuNR@mSiO$_2$ with heat treatment in SV, the rate (slope) was 0.133 min^{-1}. For AuNR@mSiO$_2$ with heat treatment in RBF, the rate was even higher, at 0.225 min^{-1}. Both were higher (5 and 10× , respectively) than the initial rate by AuNR@mSiO$_2$ without heat treatment (0.023 min^{-1}). The increased rate of reaction may be due to the increased surface areas of the gold nanostructures after CTAB ligands were removed by heat treatment. The amount of gold in all three samples was kept the same.

The results shown in Figure 11 indirectly supported the opening of pores along the body of mSiO$_2$ after heat treatment

https://doi.org/10.1021/acsomega.3c05444
ACS Omega 2023, 8, 42667−42677

in RBF because there should be more pores along the body than at the two tips, which resulted in greater rates of conversion from 4-nitrophenol to 4-aminophenol in the heat treatment of AuNR@$mSiO_2$ in RBF (red) than in SV (blue), and both were much faster than in AuNR@$mSiO_2$ without heat treatment because their pores were more clogged by CTAB ligands.

Future work includes the investigation of how to control the location of removing CTAB to open the pores. Improved optical microscopy to monitor the flow of the solution may reveal more chemistry than was known in the past. Both surface enhanced Raman spectroscopy (SERS) and NMR, especially solid-state NMR, which were employed in this work but had not yield useful information, may help elucidate the mechanisms of pore opening.[41,64−67] In addition, more reactions may be studied, given that the Au nanostructures in $mSiO_2$ are protected from coalescence and coating by unwanted surfactants, making them ideal nanostructures to catalyze without any surfactant protection.

4. CONCLUSIONS

Twelve nanostructures were made using BUTTONS from the same starting nanomaterial of AuNR@$mSiO_2$. BUTTONS stands for **b**ottom-**u**p **t**hen **to**p-dow**n** **s**ynthesis. In this work, the bottom-up portion was achieved by the solution growth of gold nanorods in mesoporous silica nanoshells (AuNR@$mSiO_2$). The top-down part was accomplished by etching AuNR@$mSiO_2$ after the nanomaterial was heat treated in different types of glassware. The control of BUTTONS was achieved with three parameters: (1) heat treatment in two different types of glassware of SVs and RBF; (2) etchant (KCN) concentrations; and (3) etching times. Depending on these parameters, different nanostructures with blue- or red-shifted plasmonic peaks were made. It is possible to expand this methodology to control the end points of syntheses when more nanostructural (such as the 12 different types of nanostructures) or spectroscopic (such as the red or blue shift of LSPR) end points are available. Optical absorption spectroscopy and microscopy as well as transmission electron microscopy were used to study the evolution of BUTTONS. These nanostructures were protected in the $mSiO_2$ and could be used to catalyze or sense without surfactant protection.

■ ASSOCIATED CONTENT

Supporting Information

The Supporting Information is available free of charge at https://pubs.acs.org/doi/10.1021/acsomega.3c05444.

Etching of CTAB-AuNRs and example of a blender generated mesh used for the DDA method simulation of AuNR@$mSiO_2$ (PDF)

■ AUTHOR INFORMATION

Corresponding Author

Ting Guo − *Department of Chemistry, University of California, Davis, California 95616, United States;* Present Address: 1520 E. Covell Suite B5-492, Davis, CA 95616; orcid.org/0000-0002-6700-0967; Email: ting1guo@gmail.com

Authors

Kristin A. Peck − *Department of Chemistry, University of California, Davis, California 95616, United States*

Jennifer Lien − *Department of Chemistry, University of California, Davis, California 95616, United States;* orcid.org/0000-0001-9244-1302

Mengqi Su − *Department of Chemistry, University of California, Davis, California 95616, United States*

Aaron D. Stacy − *Department of Chemistry, University of California, Davis, California 95616, United States*

Complete contact information is available at: https://pubs.acs.org/10.1021/acsomega.3c05444

Author Contributions

The article was written through contributions of all authors. All authors have given approval to the final version of the article.

Notes

The authors declare no competing financial interest.

■ ACKNOWLEDGMENTS

The authors thank Rong Hu, Professor Dylan Murray, and Dr. Ping Yu for their assistance.

■ REFERENCES

(1) Abid, N.; Khan, A. M.; Shujait, S.; Chaudhary, K.; Ikram, M.; Imran, M.; Haider, J.; Khan, M.; Khan, Q.; Maqbool, M. Synthesis of nanomaterials using various top-down and bottom-up approaches, influencing factors, advantages, and disadvantages: A review. *Adv. Colloid Interface Sci.* **2022**, *300*, 102597.

(2) Fu, X.; Cai, J.; Zhang, X.; Li, W. D.; Ge, H.; Hu, Y. Top-down fabrication of shape-controlled, monodisperse nanoparticles for biomedical applications. *Adv. Drug Delivery Rev.* **2018**, *132*, 169−187.

(3) de Oliveira, P. F. M.; Torresi, R. M.; Emmerling, F.; Camargo, P. H. C. Challenges and opportunities in the bottom-up mechanochemical synthesis of noble metal nanoparticles. *J. Mater. Chem. A* **2020**, *8* (32), 16114−16141.

(4) Lee, S.; Park, B.; Kim, J. S.; Kim, T. I. Designs and processes toward high-aspect-ratio nanostructures at the deep nanoscale: unconventional nanolithography and its applications. *Nanotechnology* **2016**, *27* (47), 474001.

(5) Wouters, D.; Schubert, U. S. Nanolithography and nanochemistry: probe-related patterning techniques and chemical modification for nanometer-sized devices. *Angew. Chem., Int. Ed. Engl.* **2004**, *43* (19), 2480−2495.

(6) Zhang, X. A.; Chen, I. T.; Chang, C. H. Recent progress in near-field nanolithography using light interactions with colloidal particles: from nanospheres to three-dimensional nanostructures. *Nanotechnology* **2019**, *30* (35), 352002.

(7) Liu, G.; Petrosko, S. H.; Zheng, Z.; Mirkin, C. A. Evolution of Dip-Pen Nanolithography (DPN): From Molecular Patterning to Materials Discovery. *Chem. Rev.* **2020**, *120* (13), 6009−6047.

(8) Lancaster, C. A.; Scholl, W. E.; Ticknor, M. A.; Shumaker-Parry, J. S. Uniting Top-Down and Bottom-Up Strategies Using Fabricated Nanostructures as Hosts for Synthesis of Nanomites. *J. Phys. Chem. C* **2020**, *124* (12), 6822−6829.

(9) Isaacoff, B. P.; Brown, K. A. Progress in Top-Down Control of Bottom-Up Assembly. *Nano Lett.* **2017**, *17* (11), 6508−6510.

(10) Skrabalak, S. E.; Chen, J.; Sun, Y.; Lu, X.; Au, L.; Cobley, C. M.; Xia, Y. Gold nanocages: synthesis, properties, and applications. *Acc. Chem. Res.* **2008**, *41* (12), 1587−1595.

(11) Khanal, B. P.; Zubarev, E. R. Chemical Transformation of Nanorods to Nanowires: Reversible Growth and Dissolution of Anisotropic Gold Nanostructures. *ACS Nano* **2019**, *13* (2), 2370−2378.

(12) Hauwiller, M. R.; Ye, X.; Jones, M. R.; Chan, C. M.; Calvin, J. J.; Crook, M. F.; Zheng, H.; Alivisatos, A. P. Tracking the Effects of Ligands on Oxidative Etching of Gold Nanorods in Graphene Liquid Cell Electron Microscopy. *ACS Nano* **2020**, *14* (8), 10239−10250.

(13) Zheng, Q.; Shangguan, J.; Li, X.; Zhang, Q.; Bustillo, K. C.; Wang, L. W.; Jiang, J.; Zheng, H. Observation of Surface Ligands-Controlled Etching of Palladium Nanocrystals. *Nano Lett.* **2021**, *21* (15), 6640−6647.
(14) Wang, W.; Xu, T.; Bai, T.; Zhu, C.; Zhang, Q.; Zhang, H.; Zhang, H.; Guo, Z.; Zheng, H.; Sun, L. Controlled oxidative etching of gold nanorods revealed through in-situ liquid cell electron microscopy. *Sci. China Mater.* **2020**, *63* (12), 2599−2605.
(15) Yuan, H.; Janssen, K. P. F.; Franklin, T.; Lu, G.; Su, L.; Gu, X.; Uji-i, H.; Roeffaers, M. B. J.; Hofkens, J. Reshaping anisotropic gold nanoparticles through oxidative etching: the role of the surfactant and nanoparticle surface curvature. *RSC Adv.* **2015**, *5* (9), 6829−6833.
(16) Free, P.; Conger, G.; Siji, W.; Zhang, J. B.; Fernig, D. G. High colloidal stability of gold nanorods coated with a peptide-ethylene glycol: Analysis by cyanide-mediated etching and nanoparticle tracking analysis. *Colloids Surf., B* **2016**, *146*, 871−878.
(17) Kermanshahian, K.; Yadegar, A.; Ghourchian, H. Gold nanorods etching as a powerful signaling process for plasmonic multicolorimetric chemo-/biosensors: Strategies and applications. *Coord. Chem. Rev.* **2021**, *442*, 213934.
(18) Ye, X.; Zheng, C.; Chen, J.; Gao, Y.; Murray, C. B. Using binary surfactant mixtures to simultaneously improve the dimensional tunability and monodispersity in the seeded growth of gold nanorods. *Nano Lett.* **2013**, *13* (2), 765−771.
(19) Nikoobakht, B.; El-Sayed, M. A. Preparation and Growth Mechanism of Gold Nanorods NRs) Using Seed-Mediated Growth Method. *Chem. Mater.* **2003**, *15* (10), 1957−1962.
(20) Johnson, C. J.; Dujardin, E.; Davis, S. A.; Murphy, C. J.; Mann, S. Growth and form of gold nanorods prepared by seed-mediated, surfactant-directed synthesis. *J. Mater. Chem.* **2002**, *12* (6), 1765−1770.
(21) Kim, F.; Song, J. H.; Yang, P. Photochemical synthesis of gold nanorods. *J. Am. Chem. Soc.* **2002**, *124* (48), 14316−14317.
(22) Yu; Chang, S.-S.; Lee, C.-L.; Wang, C. R. C. Gold nanorods: Electrochemical synthesis and optical properties. *J. Phys. Chem. B* **1997**, *101* (34), 6661−6664.
(23) Jana, N. R.; Gearheart, L.; Obare, S. O.; Murphy, C. J. Anisotropic Chemical Reactivity of Gold Spheroids and Nanorods. *Langmuir* **2002**, *18* (3), 922−927.
(24) Rodriguez-Fernandez, J.; Perez-Juste, J.; Mulvaney, P.; Liz-Marzan, L. M. Spatially-directed oxidation of gold nanoparticles by Au(III)-CTAB complexes. *J. Phys. Chem. B* **2005**, *109* (30), 14257−14261.
(25) Lee, S.; Nam, Y.-S.; Choi, S.-H.; Lee, Y.; Lee, K.-B. Highly sensitive photometric determination of cyanide based on selective etching of gold nanorods. *Microchim. Acta* **2016**, *183* (11), 3035−3041.
(26) Tsung, C. K.; Kou, X.; Shi, Q.; Zhang, J.; Yeung, M. H.; Wang, J.; Stucky, G. D. Selective shortening of single-crystalline gold nanorods by mild oxidation. *J. Am. Chem. Soc.* **2006**, *128* (16), 5352−5353.
(27) Lu, S.; Chen, L.; Yang, P.; Matras-Postolek, K. Highly sensitive visual detection of catalase based on the accelerating decomposition of H2O2 using Au nanorods as a sensor. *RSC Adv.* **2016**, *6* (23), 19620−19625.
(28) Zhang, Z.; Chen, Z.; Pan, D.; Chen, L. Fenton-like reaction-mediated etching of gold nanorods for visual detection of Co(2+). *Langmuir* **2015**, *31* (1), 643−650.
(29) Weng, G.; Dong, X.; Li, J.; Zhao, J. Halide ions can trigger the oxidative etching of gold nanorods with the iodide ions being the most efficient. *J. Mater. Sci.* **2016**, *51* (16), 7678−7690.
(30) Wen, T.; Zhang, H.; Tang, X.; Chu, W.; Liu, W.; Ji, Y.; Hu, Z.; Hou, S.; Hu, X.; Wu, X. Copper Ion Assisted Reshaping and Etching of Gold Nanorods: Mechanism Studies and Applications. *J. Phys. Chem. C* **2013**, *117* (48), 25769−25777.
(31) Zheng, J.; Cheng, X.; Zhang, H.; Bai, X.; Ai, R.; Shao, L.; Wang, J. Gold Nanorods: The Most Versatile Plasmonic Nanoparticles. *Chem. Rev.* **2021**, *121* (21), 13342−13453.
(32) Wu, Z.; Liang, Y.; Guo, Q.; Zhang, K.; Liang, S.; Yang, L.; Xiao, Q.; Wang, D. Study on selective oxidations of gold nanorod and mesoporous silica-coated gold nanorod. *J. Mater. Sci.* **2019**, *54* (11), 8133−8147.
(33) Rao, H.; Xue, X.; Wang, H.; Xue, Z. Gold nanorod etching-based multicolorimetric sensors: strategies and applications. *J. Mater. Chem. C* **2019**, *7* (16), 4610−4621.
(34) Zhang, Z.; Wang, H.; Chen, Z.; Wang, X.; Choo, J.; Chen, L. Plasmonic colorimetric sensors based on etching and growth of noble metal nanoparticles: Strategies and applications. *Biosens. Bioelectron.* **2018**, *114*, 52−65.
(35) Bao, Z.; Sun, Z.; Xiao, M.; Chen, H.; Tian, L.; Wang, J. Transverse oxidation of gold nanorods assisted by selective end capping of silver oxide. *J. Mater. Chem.* **2011**, *21* (31), 11537.
(36) Carattino, A.; Khatua, S.; Orrit, M. In situ tuning of gold nanorod plasmon through oxidative cyanide etching. *Phys. Chem. Chem. Phys.* **2016**, *18* (23), 15619−15624.
(37) Xie, F.; Ye, W.; Sun, H.; Kou, S.; Guo, X. Silver Ions Induce Lateral Etching of Gold Nanorods by K2PtCl4. *Langmuir* **2015**, *31* (24), 6823−6828.
(38) Thambi, V.; Kar, A.; Ghosh, P.; Khatua, S. Light-Controlled in Situ Bidirectional Tuning and Monitoring of Gold Nanorod Plasmon via Oxidative Etching with FeCl3. *J. Phys. Chem. C* **2018**, *122* (43), 24885−24890.
(39) Hauwiller, M. R.; Ondry, J. C.; Chan, C. M.; Khandekar, P.; Yu, J.; Alivisatos, A. P. Gold Nanocrystal Etching as a Means of Probing the Dynamic Chemical Environment in Graphene Liquid Cell Electron Microscopy. *J. Am. Chem. Soc.* **2019**, *141* (10), 4428−4437.
(40) Xiang, Y.; Wu, X.; Liu, D.; Feng, L.; Zhang, K.; Chu, W.; Zhou, W.; Xie, S. Tuning the Morphology of Gold Nanocrystals by Switching the Growth of {110} Facets from Restriction to Preference. *J. Phys. Chem. C* **2008**, *112* (9), 3203−3208.
(41) Janicek, B. E.; Hinman, J. G.; Hinman, J. J.; Bae, S. H.; Wu, M.; Turner, J.; Chang, H. H.; Park, E.; Lawless, R.; Suslick, K. S.; Murphy, C. J.; Huang, P. Y. Quantitative Imaging of Organic Ligand Density on Anisotropic Inorganic Nanocrystals. *Nano Lett.* **2019**, *19* (9), 6308−6314.
(42) Wu, Z.; Zeng, Q.; Wang, H. Structural controls of AuNR@mSiO2: tuning of the SPR, and manipulation of the silica shell thickness and structure. *J. Mater. Chem. C* **2016**, *4* (13), 2614−2620.
(43) Deng, T.-S.; van der Hoeven, J. E. S.; Yalcin, A. O.; Zandbergen, H. W.; van Huis, M. A.; van Blaaderen, A. Oxidative Etching and Metal Overgrowth of Gold Nanorods within Mesoporous Silica Shells. *Chem. Mater.* **2015**, *27* (20), 7196−7203.
(44) Takahata, R.; Yamazoe, S.; Warakulwit, C.; Limtrakul, J.; Tsukuda, T. Rayleigh Instability and Surfactant-Mediated Stabilization of Ultrathin Gold Nanorods. *J. Phys. Chem. C* **2016**, *120* (30), 17006−17010.
(45) Thapa, D. K.; Pandey, A. Cloning nanocrystal morphology with soft templates. *Chem. Phys. Lett.* **2016**, *658*, 315−318.
(46) Brioude, A.; Jiang, X. C.; Pileni, M. P. Optical properties of gold nanorods: DDA simulations supported by experiments. *J. Phys. Chem. B* **2005**, *109* (27), 13138−13142.
(47) Gorelikov, I.; Matsuura, N. Single-step coating of mesoporous silica on cetyltrimethyl ammonium bromide-capped nanoparticles. *Nano Lett.* **2008**, *8* (1), 369−373.
(48) Mohanta, J.; Satapathy, S.; Si, S. Porous Silica-Coated Gold Nanorods: A Highly Active Catalyst for the Reduction of 4-Nitrophenol. *ChemPhysChem* **2016**, *17* (3), 364−368.
(49) Draine, B. T.; Flatau, P. J. Discrete-Dipole Approximation For Scattering Calculations. *J. Opt. Soc. Am. A* **1994**, *11* (4), 1491−1499.
(50) Johnson, P. B.; Christy, R. W. Optical Constants of the Noble Metals. *Phys. Rev. B* **1972**, *6* (12), 4370−4379.
(51) Feng, J.; Wang, Z.; Shen, B.; Zhang, L.; Yang, X.; He, N. Effects of template removal on both morphology of mesoporous silica-coated gold nanorod and its biomedical application. *RSC Adv.* **2014**, *4* (54), 28683−28690.

https://doi.org/10.1021/acsomega.3c05444
ACS Omega 2023, 8, 42667−42677

(52) Zhu, X.; Xu, J.; Yun, Q.; Wang, C.; Ruan, Q.; Kan, C. Realization of red plasmon shifts by the selective etching of Ag nanorods. *CrystEngComm* **2020**, *22* (45), 7870−7876.
(53) Stefan Kooij, E.; Poelsema, B. Shape and size effects in the optical properties of metallic nanorods. *Phys. Chem. Chem. Phys.* **2006**, *8* (28), 3349−3357.
(54) Ungureanu, C.; Rayavarapu, R. G.; Manohar, S.; van Leeuwen, T. G. Discrete dipole approximation simulations of gold nanorod optical properties: Choice of input parameters and comparison with experiment. *J. Appl. Phys.* **2009**, *105* (10), 102032.
(55) Sosa, I. O.; Noguez, C.; Barrera, R. G. Optical Properties of Metal Nanoparticles with Arbitrary Shapes. *J. Phys. Chem. B* **2003**, *107* (26), 6269−6275.
(56) Min, C.; Meng, W.; Ning, G. Calculated Optical Properties of Dielectric Shell Coated Gold Nanorods. *Chin. Phys. Lett.* **2009**, *26* (4), 045201.
(57) Green, T. A. Gold etching for microfabrication. *Gold Bull.* **2014**, *47* (3), 205−216.
(58) Adelt, M.; MacLaren, D. A.; Birch, D. J. S.; Chen, Y. Morphological Changes of Silica Shells Deposited on Gold Nanorods: Implications for Nanoscale Photocatalysts. *ACS Appl. Nano Mater.* **2021**, *4* (8), 7730−7738.
(59) Zeng, J.; Zhang, Q.; Chen, J.; Xia, Y. A comparison study of the catalytic properties of Au-based nanocages, nanoboxes, and nanoparticles. *Nano Lett.* **2010**, *10* (1), 30−35.
(60) Wu, H.; Wu, Z.; Liu, B.; Zhao, X. Can. Plasmonic Effect Cause an Increase in the Catalytic Reduction of p-nitrophenol by Sodium Borohydride over Au Nanorods? *ACS Omega* **2020**, *5* (21), 11998−12004.
(61) Bai, X.; Gao, Y.; Liu, H.-g.; Zheng, L. Synthesis of Amphiphilic Ionic Liquids Terminated Gold Nanorods and Their Superior Catalytic Activity for the Reduction of Nitro Compounds. *J. Phys. Chem. C* **2009**, *113* (41), 17730−17736.
(62) Kundu, S.; Lau, S.; Liang, H. Shape-Controlled Catalysis by Cetyltrimethylammonium Bromide Terminated Gold Nanospheres, Nanorods, and Nanoprisms. *J. Phys. Chem. C* **2009**, *113* (13), 5150−5156.
(63) Zhao, P.; Feng, X.; Huang, D.; Yang, G.; Astruc, D. Basic concepts and recent advances in nitrophenol reduction by gold- and other transition metal nanoparticles. *Coord. Chem. Rev.* **2015**, *287*, 114−136.
(64) Wu, M.; Vartanian, A. M.; Chong, G.; Pandiakumar, A. K.; Hamers, R. J.; Hernandez, R.; Murphy, C. J. Solution NMR Analysis of Ligand Environment in Quaternary Ammonium-Terminated Self-Assembled Monolayers on Gold Nanoparticles: The Effect of Surface Curvature and Ligand Structure. *J. Am. Chem. Soc.* **2019**, *141* (10), 4316−4327.
(65) Gao, Z.; Burrows, N. D.; Valley, N. A.; Schatz, G. C.; Murphy, C. J.; Haynes, C. L. In solution SERS sensing using mesoporous silica-coated gold nanorods. *Analyst* **2016**, *141* (17), 5088−5095.
(66) Kang, H.; Haynes, C. Interactions between Silica-Coated Gold Nanorod Substrates and Hydrophobic Analytes in Colloidal Surface-Enhanced Raman Spectroscopy. *J. Phys. Chem. C* **2019**, *123* (40), 24685−24697.
(67) van der Hoeven, J. E. S.; Deng, T. S.; Albrecht, W.; Olthof, L. A.; van Huis, M. A.; de Jongh, P. E.; van Blaaderen, A. Structural Control over Bimetallic Core-Shell Nanorods for Surface-Enhanced Raman Spectroscopy. *ACS Omega* **2021**, *6* (10), 7034−7046.

https://doi.org/10.1021/acsomega.3c05444
ACS Omega 2023, 8, 42667−42677